CrossMark

A comparative TCAD simulations of a P-and N-type organic field effect transistors: field-dependent mobility, bulk and interface traps models

A. Boubaker[1] · B. Hafsi[1,2] · K. Lmimouni[2] · A. Kalboussi[1]

Abstract Pentacene and Polyera™ N2200 based-organic field effect transistors (OFETs), have been fabricated and simulated in a bottom-gate/back contacts configuration. The simulations were processed with the help of 2D drift–diffusion model. Comparison and analysis of the electrical characteristics of both n- and p-channel OFETs have been investigated. The study was centred on the electrical performance of every structure in term of mobility, fixed charge at the oxide/semiconductor interface and bulk traps density and its related energy. The dependence of the transfer characteristic on the grain boundaries traps state, in the case of pentacene, has been also outlined. Comparison between the simulation results and our experimental data show a good agreement. We finally present how our model can be applied to different devices with different channel length and we analyse their relationship with extracted electrical parameters.

1 Introduction

Organic electronic components are promising candidates for the next generation electronics due to their solution processability, structural versatility by molecular design, and their appealing mechanical properties making flexible electronics a reality [1]. Various types of organic electronic device, such as solar cells [2], light-emitting diodes [3],

field-effect transistors (OFETs) and sensors [4] have been fabricated. In recent years, Organic field-effect transistors show a considerable development because of their low manufacturing costs, their power consumption and the possibility to fabricate electronic devices performing simple operations or functions such as inverter and ring oscillators [5].

On the other hand, the variety of synthetic organic chemistry has enabled the engineering of both *n*- and *p*-type semiconductors, giving rise to many potential candidates for circuit designs based on CMOS technology [6]. The study of the charge transport in these materials is therefore very important for the development of organic devices and the optimizing of their characteristics. It is therefore critical that the research in this area is necessarily be coupled with theoretical perspective, in order to resolve several of the important issues, which will help in further enhancing the electrical properties of these devices.

The basic idea of this paper is defended by simulation and comparison between two stable n- and p-type materials, pentacene and Polyera™ N2200, respectively. We analyse the differences between the two types of transistors, in terms of the electrical properties and the influences caused by structural changes. For this, we use a 2D drift–diffusion simulator Integrated System Engineering-Technology Computer Aided Design (ISE-TCAD®).

1.1 Structures and operating principal

We address the influence of mobility on the OTFTs electrical characteristics and the interplay between bulk traps states and fixed charges at the oxide/semiconductor Interface. As a reference, we will compare the simulated characteristics of both types of OTFTs to those realized by our group. The dependence of the transfer characteristic on

✉ B. Hafsi
bilel.hafsi@iemn.univ-lille1.fr

[1] University of Monastir, Microelectronics and instrumentation laboratory, Av de l'environnement, 5019 Monastir, Tunisia

[2] University of Lille, IEMN Laboratory, Avenue Poincaré 59652 Villeneuve d'Ascq Cedex, France

the grain boundaries traps state, in the case of pentacene, will be also considered. OFETs devices were fabricated in a (Back Gate/ Bottom Contact) configuration on heavily doped Si wafer featuring a 200 nm SiO_2 layer with patterned 30 nm Au electrodes (Fig. 1). The electrodes set involved different channel lengths (5, 10, 20 and 50 μm) and a 1 mm width. Substrates were rinsed with acetone, isopropanol followed by ultraviolet irradiation using UV-ozone cleaning for 30 min. We use piranha solution (H_2SO_4/H_2O_2, 2/1 v/v) for 15 min (Caution: preparation of the piranha solution is highly exothermic and reacts violently with organics), then we rinse with DI water. Finally, a layer of [P (NDI2ODT2)] (n-type polymer obtained from Polyera™ company) was spin coated from chloroform solution and annealed at 120 °C for 18 h in a glove box filled with high-purity nitrogen for the n-type devices and a thin layer of pentacene (about 30 nm at a deposition rate of 0.1 Å/s) (molecules obtained from Sigma Aldrich) was sublimated (in vacuum atmosphere, 10^{-6} mbar) for the p-type devices. The electronic characteristics of both types of transistors were tested with a probe station using a computer-controlled Agilent 4156 in a dry nitrogen glove box (O_2 and H_2O <1 ppm) with a single sweep current I versus voltage V characteristics.

A voltage is applied to the gate in order to control the amount of current flow between the source and drain. The gate controls the MOS capacitor by accumulating or rejecting the charge carriers, which in turn activates or deactivates the transistor.

Since the lowest unoccupied molecular orbital (LUMO) is completely empty and the highest occupied molecular orbital (HOMO) is filled, the semiconductor is in the energy situation of an insulator (Fig. 2a). This situation will continue as long as the voltage V_{GS} is not sufficient to bring the levels of the two bands, HOMO or LUMO, in resonance with the electrodes Fermi level. The application of a sufficient positive gate will bring the LUMO band next to the electrodes Fermi level, leading to an ohmic contacts, which will allow the electrodes to fill the LUMO band with electrons (Fig. 2b). In this case, electrons are accumulated in the semiconductor.

Once a small potential V_{DS} is applied between the source and the drain, electrons move throw the semiconductor by the electric field effect (Fig. 2d). This is the operation mechanism in n channel. However, in the case of a p-type semiconductor, when a negative voltage V_{GS} is applied to the gate (Fig. 2c), the energy levels of the semiconductor bands increase so the HOMO band will be next to the electrodes Fermi level, creating holes accumulation. When V_{DS} <0 is applied, holes (positive charges), transport appears (Fig. 2e).

2 Comparative simulations and OFETs performances

2.1 Simulation model

The TCAD process plays a critical role in advanced technology development by giving insight into the relationships between processing and nanoscale performance that cannot be obtained from compact and circuit simulation tools [7]. ISE-TCAD is a finite-element analysis that has application-specific modules for various physics phenomena. It consists of a multitude of core products for two and three-dimensional processes integrated into a powerful interface.

In this work, the structure used in the ISE-TCAD input file has a channel length of 5 μm with a W/L ratio of about 200.

Fig. 1 Schematic structure of bottom gate/back contact OFET, the organic semiconductors are pentacene and PolyeraTM N2200
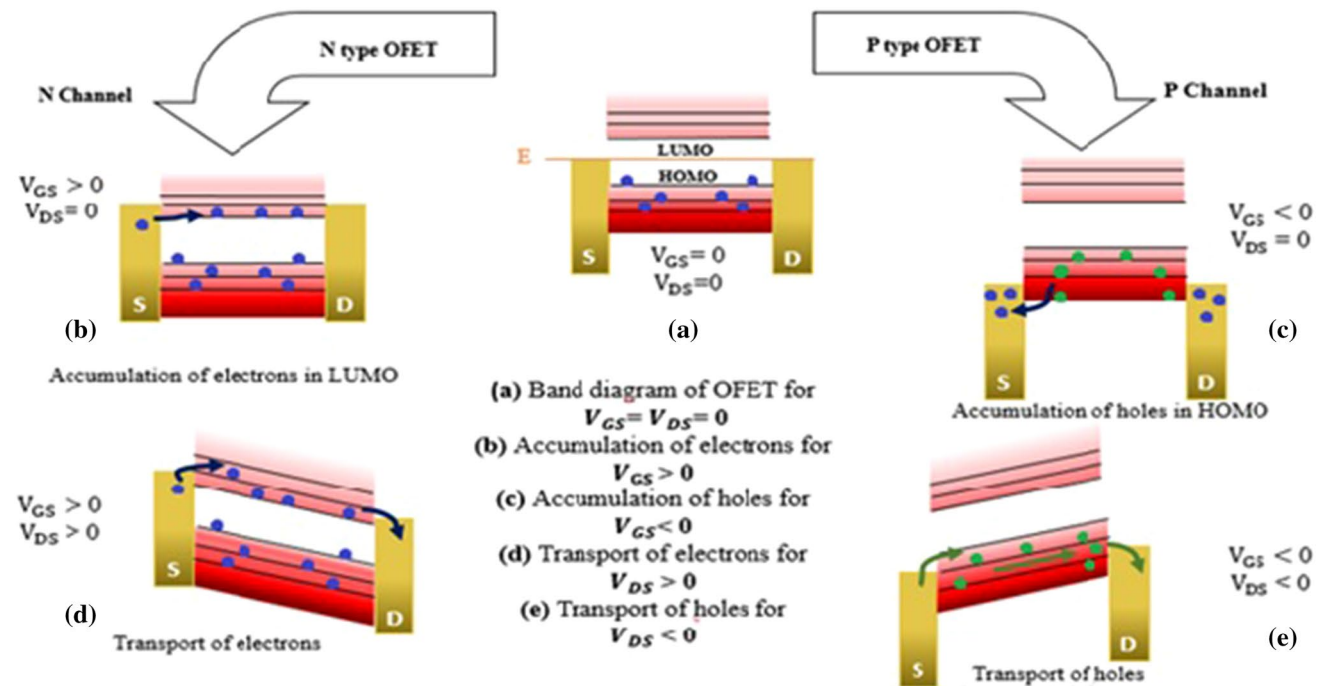
(a)

(b) Pentacene
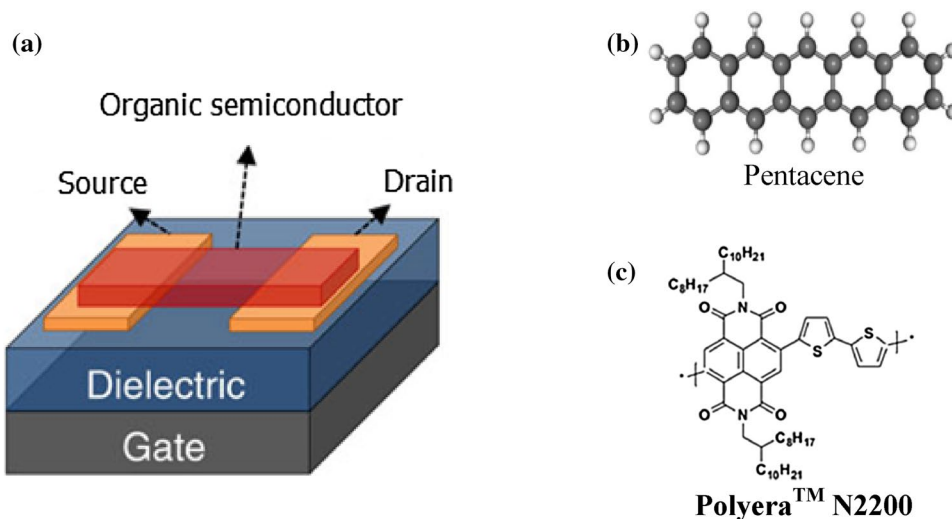
(c) **Polyera^{TM} N2200**

Fig. 2 Comparison of band diagrams between n and p-Type OFETs

A thin layer about 30 nm of pentacene (120 nm PolyeraT^M N2200) was considered as an active layer. ISE-TCAD is amply used right from the start device structure construction, transistor modelling, followed by a process flow and finally plotting the electrical characteristics. A finite element solver finds a coupled solution of Poisson and drift–diffusion equations for electrons and holes. The Poisson equation allows the description of the evolution of the field in terms of carrier densities. Reduced to the electrostatic potential, it provides the following equation:

$$\Delta V = -\frac{\rho(x, y, z)}{\varepsilon} \tag{1}$$

where ε and ρ are the semiconductor permittivity and carriers density in the semiconductor, respectively.

The continuity equations reflect the change in the carrier density over time, which is due to the difference between the incoming and outgoing flux of carriers adding the generation and minus the recombination [8]. Charge conservation then is applied through the equations (2) and (3), one for electrons and one for holes.

$$\frac{\partial n}{\partial t} = \frac{1}{q} \cdot div\vec{J_n} + G_n - R_n \tag{2}$$

$$\frac{\partial p}{\partial t} = -\frac{1}{q} \cdot div\vec{J_p} + G_p - R_p \tag{3}$$

where G_n, G_p, R_n and R_p are the generation and recombination rates of electrons and holes respectively.

The Poisson equation and the continuity equations provide the necessary simulation for all components bases. Electrons and holes current are described as the sum of two contributions and a component proportional to the diffusion gradient of the carrier density.

$$\vec{J_n} = qn\mu_n\vec{E_n} + qD_n\overrightarrow{grad}n \tag{4}$$

$$\vec{J_p} = qn\mu_p\vec{E_p} - qD_p\overrightarrow{grad}p \tag{5}$$

where D_n and D_p are the Einstein diffusion coefficients for low carriers density, they are related to the temperature and mobility by the well-known laws:

$$D_n = \frac{kT}{q}\mu_n \tag{6}$$

$$D_p = \frac{kT}{q}\mu_p \tag{7}$$

The Einstein relation has so far been applied for high-density crystalline-semiconductors or degenerate-semiconductors with a band tail distribution [9]. In our simulation, generalized Einstein relation is solved for a Gaussian density of states [9], as always used for organic semiconductors and other amorphous semiconductors like polymers.

Our simulation flow includes the interface (MDRAW) that defines the device architecture, the different types of materials, meshing engine, and the doping profiles especially for the active layer (Pentacene, Polyera™ N2200). The potential across the channel is set by two boundary conditions set at the source and at the drain. In our simulations, electrodes have voltage boundary conditions with the initial condition of zero bias. For metal–semiconductor interfaces, by default, there is an Ohmic boundary condition that can be written as: .

$$\vec{j}_M \cdot \hbar = \left(\vec{j}_n + \vec{j}_p + \vec{j}_D \right) \cdot \hbar \ (8)$$

$$\left\{ \begin{array}{r} \psi = \psi_M + \psi_0 \\ n = n_0 \\ p = p_0 \end{array} \right\} \quad (8)$$

where ψ_0 is the equilibrium electrostatic potential, n_0 and p_0 are the electron and hole equilibrium concentration and $\vec{j}_n$ and $\vec{j}_p$ are the electron and the hole current at the semiconductor side of the interface.

In organic semiconductors, charge transport is mainly controlled by jumps between localized states which are induced by the disorder. The probability of jump and mobility depends on the electric field [11]. The field mobility is defined by the Poole–Frenkel mobility which defines the dependency of mobility to the electric field. This model is expressed as [8]:

$$\mu(E) = \mu_0 \exp \left(-\frac{\Delta}{KT} + \left(\frac{\beta}{KT} - \gamma \right) \sqrt{E} \right) \quad (9)$$

where μ_0, E, Δ, β, γ, K and T are respectively the zero field mobility, the electrical field, the zero field activation energy, the Pool–Frenkel factor, a fitting parameter, the Boltzmann constant and the room temperature. The used parameters values for pentacene and Polyera™ N2200 in

this study are summarized in Table 1. The parameter related to the materials disorder is the temperature. Near room temperature, the field dependence of the mobility is often reasonably described by an effective Poole–Frenkel model of mobility. At low temperatures and large gate voltages, transport in materials becomes nearly temperature independent, crossing over into a regime described by field-driven tunnelling [10].

The drain current in organic transistor is conventionally cited in literature using classic theory of inorganic transistors [25]:

$$I_d = \left\{ \begin{array}{l} \dfrac{w}{2L} C_i \mu (V_{gs} - V_{th}) \ if \ \left| V_{gs} - V_{th} \right| > \left| V_{ds} \right| > 0 \\[2ex] \dfrac{w}{L} C_i \mu (V_{gs} - V_{th}) V_{ds} \ if \ \left| V_{ds} \right| > \left| V_{gs} - V_{th} \right| > 0 \end{array} \right.$$

where w, L, C_i and V_{th} are respectively the channel width, channel length, capacitance of the gate insulator per unit area, mobility and threshold voltage.

The extracted field effect mobility is obtained in the saturation region by

$$\mu_{sat} = \frac{2L}{WC} \left(\frac{\partial \sqrt{I_D}}{\partial V_{gs}} \right)^2 \quad (10)$$

equation (10) [25]:

The sub-threshold is determined from the theoretical Eq. [26]:

$$S = \frac{\partial V_{GS}}{\partial \left(\log \left(I_{DS} \right) \right)} \quad (11)$$

where S is the calculated slope of the trans-characteristic. Here, V_{GS} and I_{DS} are the gate voltage and the drain current, respectively. Note that the smaller value of S is required for the higher operating speed [27].

Table 1 Summary of the physical and energetic parameters of pentacene and N2200

Propriété	Symbole	Materials		Unit
		Pentacene	Polyera™	
HOMO		−4.6	−5,4	eV
LUMO		−2.35	−4	eV
Gap	E_g	2.25 [11]	1.4 [13]	eV
Electronic affinity	χ	2.49 [12]	4 [14]	eV
intrinsic Concentration	N_i	2.5×10^{17} [15]	10^{10} [16]	cm^{-3}
Permittivity	ε	4 [17]	3.5 [18]	
Traps density	N_t	10^{17} [19]	3×10^{18} [20]	cm^{-3}
Traps energy	E_0	0.19 [19]	0.04 [20]	eV
Low field mobility	μ_0	3.3×10^{-3} [21]	5×10^{-4} [22]	cm^{2}V^{-1}s^{-1}
Effective densities of states	N_C	3×10^{21}	10^{21}	cm^{-3}
	N_V	3×10^{21} [23]	10^{21} [24]	cm^{-3}

2.2 Results and discussions

To describe the charge transport in our organic devices we have defined some models: (1) semiconductor density of traps (2) trap model at the interface between semiconductor and oxide (3) fixed charges (4) charge mobility. Several simulations have been carried out to calculate the behaviour of OFET's.

In the following we will consider the influence of the mobility model on the electrical characteristics, we will compare simulations made with a constant mobility model and those made with a field dependent mobility model. Using the parameters given in Table 1, the simulated I_{DS}-V_{DS} characteristics of pentacene based-OFET for a constant mobility model are shown in Fig. 2. The gate voltage is fixed at −10, −20, −30 and −40V while the drain voltage (V_{DS}) range from 0 to −40 V in a step of −0.5 V. When we apply a negative voltage between the drain and the source, a holes flow from the source to the drain causing a negative current flowing appears. As the magnitude of the drain-source voltage is increased, the value of the drain-source current also increases until "pinch-off" at which point the p-channel pinches closed one side and the drain current saturates at its maximum value. Output characteristics of our pentacene based transistors obtained from simulation and experimental data are shown in Fig. 3.

The curves show saturation zones for high V_{DS} drain voltages, but we can be easily observe an overestimation of the drain current in the linear region for low drain voltages. Therefore, the need for a field-dependent mobility model is important to better describe the electrical behaviour of an organic material

The presence of field dependent mobility in pentacene based OTFTs is shown by the output characteristics of devices with L = 5 µm as shown in Fig. 4. We note that this (Pool Frenkel) field-dependence is always observed in disordered organic semiconductors. In this respect, the field-dependence mobility given by Eq. (9) is incorporated in our simulation, in addition to the contact barrier effect. The best fit to the experimental data is obtained with $\mu_0 = 3.3 \times 10^{-3}$ cm^2 V^{-1} s^{-1}, $\beta = 1.45 \times 10^{-5}$ eV (cm/V)$^{1/2}$, $\gamma = 10^{-5}$ (cm/V)$^{1/2}$, respectively. However, the agreement between simulation and experiment is not yet reached. The shift in the curves can be improved by taking into account the bulk traps densities and their associated energies. The trapped charge consists of both donor-like and acceptor-like states across the forbidden energy gap. The density of defect states, g (E), is defined as a combination of four components: Two tail bands with an exponentially decreasing function are specified to contain large numbers of defect states at the conduction and valence band edges, respectively and two deep-level bands for acceptor-and donor-like defects which are defined as a Gaussian distribution [8].

$$g_{GA}(E) = N_{GA} \exp \left[-\left(\frac{E - E_{GA}}{W_{GA}} \right)^2 \right] \quad (12)$$

We used a single Acceptor level traps (neutral if empty, negative if occupied by an electron) in the semiconductors bulk. The trap is characterized by the energy level, representing the difference between the defect energy level and valence band energy (HOMO) in the case of pentacene or conduction band (LUMO) in the case of Polyera™ N2200, and the concentration of electron trapped on the energy level. It has also been found
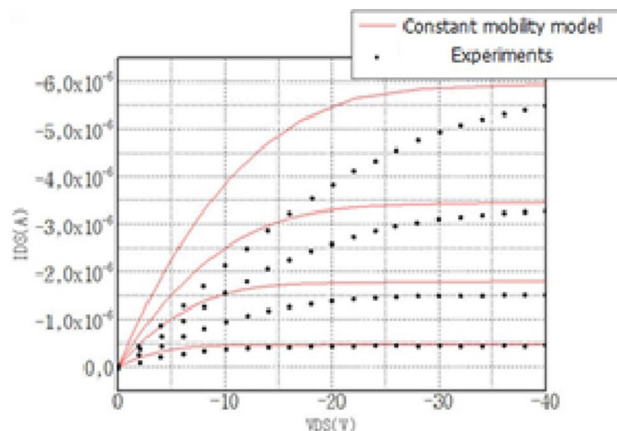

Fig. 3 IDS–VDS characteristics based on a constant mobility model compared with experimental data for pentacene OFET
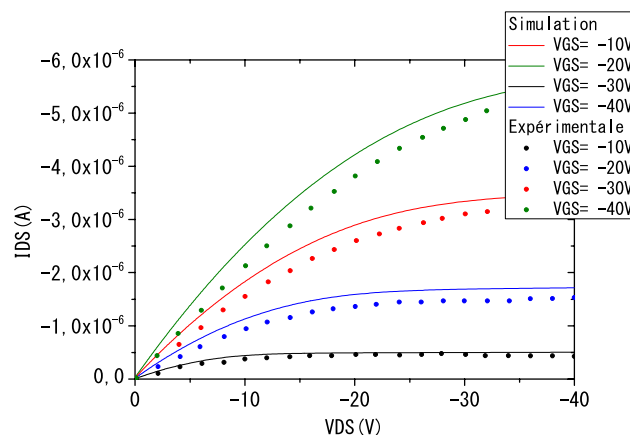

Fig. 4 IDS–VDS characteristics based on a field dependent-mobility model compared with experimental data for pentacene OFET, W/L = 200

that the transfer characteristic of an organic thin film transistor is greatly affected by traps states and fixed charges present at the interface between the oxide and semiconductor. In particular, traps present at the interface
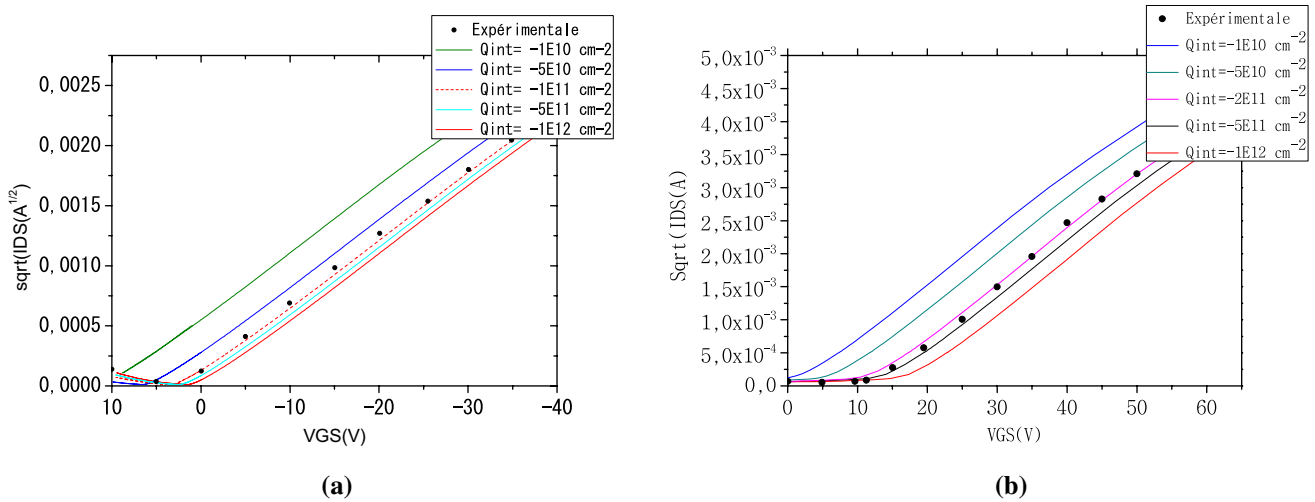
Fig. 5 Experimental transfer characteristics and simulation result for different fixed charges concentrations at the semiconductor/oxide interface **a** for pentacene based-OFET **b** for Polyera™ N2200 based-OFET, W/L = 200

between oxide and semiconductor has an influence on the transistor transfer characteristics in the subthreshold region, while the threshold voltage is governed by the fixed charges present at this interface according to the relationship [28, 29]:

$$\Delta V_{th} = -\frac{Q_{int}}{C_{OX}} \tag{13}$$

Figure 5a shows the dependence of the transfer characteristics to the variation of fixed charges at the semiconductor/oxide interface. It is noted that increasing the concentration of fixed charges has the effect of shifting the threshold voltage towards high values (absolute values). Thus comparing the experimental curves with those simulated for both types of transistor, one is able to determine the concentration of fixed charges which provide a best fit with the experimental results. For our devices, there is $Q_{int} = -1 \times 10^{11}$ cm^{-2} which induces threshold voltage $V_{th} = 12.9$ V for pentacene-based OFET and $Q_{int} = -2 \times 10^{11}$ cm^{-2} with $V_{th} = 10$ V for Polyera™ N2200 based transistor. We have then considered the influence of bulk traps. In particular the influence of the acceptor trap concentration and there concentration on the subthreshold trans-characteristic slope. In the following, we will consider a single acceptor trap level inside the forbidden band and we will analyse its effects of varying both the concentration and the energy level from the valence band and the conduction band for both pentacene and Polyera™ N2200, respectively. Figure 6 shows the trans-characteristics obtained by varying trap

concentrations. ISE-TCAD simulates the effect of trap densities near the valence band in the case of pentacene. For an average energy of about 0.19 eV, simulations of output characteristics for different traps concentrations (with a gate voltage $V_{GS} = 30$ V) (Fig. 6a), show a strong dependence of the output current, a value between 10^{17} cm^{-3} and 5×10^{17} cm^{-3} shows a good agreement in saturation mode with the experimental transistor characteristic. An average value of 2.5×10^{17}cm^{-3} will be considered in the following simulations. Figure 6b illustrates the output characteristics of an pentacene based OFET for different energy values of hole traps with a bias $V_{DS} = -30$V and a bulk density of traps fixed at $N_{traps} = 2.5 \times 10^{17}$cm^{-3}. As expected, by increasing the energy level of traps towards the valence band, the effect of traps decreases and the value of the slope below the threshold, thus approaching behaviour without traps effect. From the above analysis, it is concluded that the effect of the traps is sufficiently represented by a single level of traps with an energy equal to 0.2 eV beyond the valence band with a concentration equal to 2.5×10^{17}cm^{-3}. The same methodology was followed to simulate the electrical characteristics of the Polyera™ N2200 based transistor as function as he traps concentration and their energy beyond the conduction band (Fig. 6c, d).

The simulation result shows also a saturation current dependence, in particular, by increasing the concentration of acceptors traps, the current value decreases. We note that the best agreement between the simulated and experimental I–V characteristics has been obtained for a trap density 10^{18} cm^{-3} and energy of about 0.05 eV beyond the

(a)
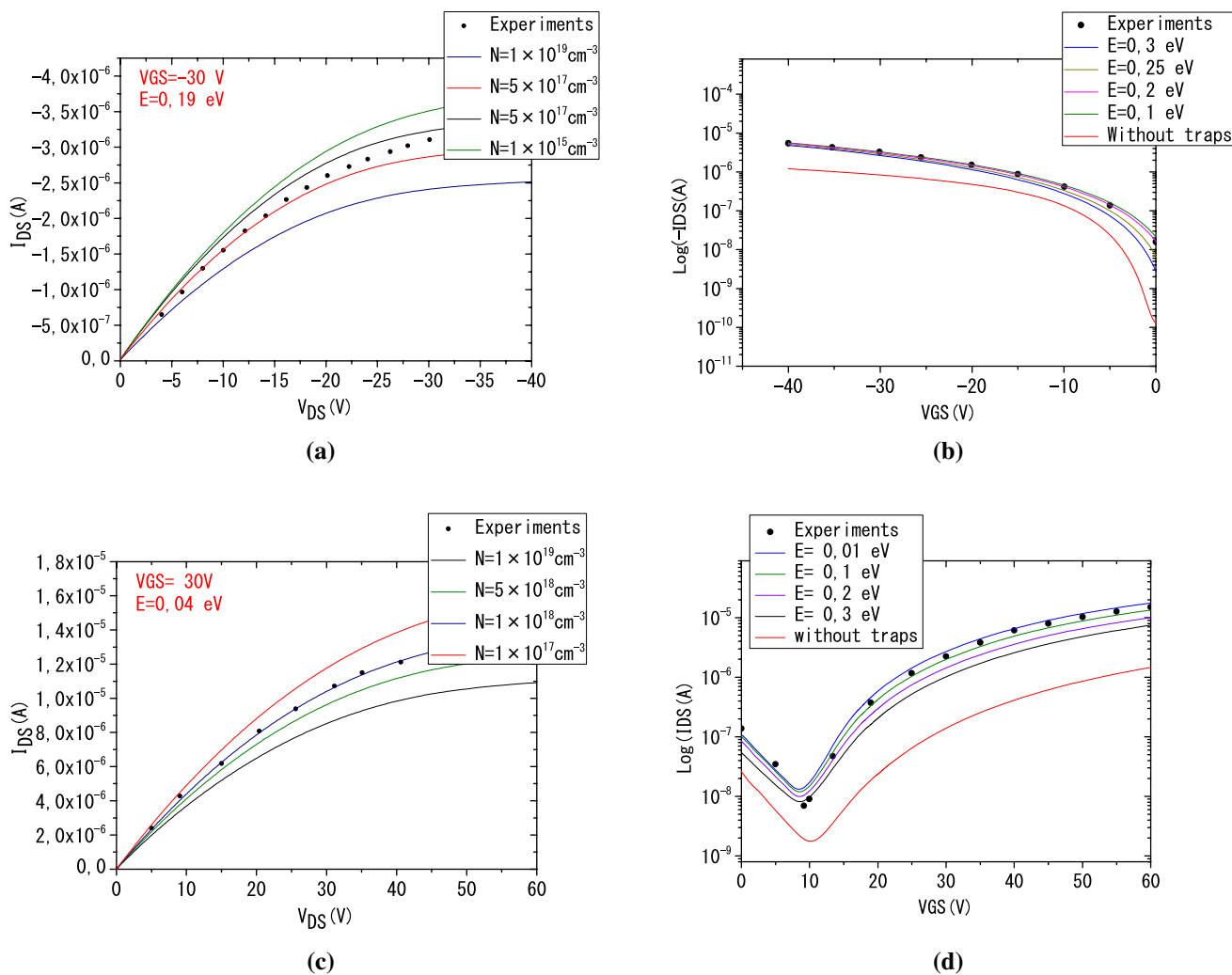

(b)

(c)

(d)

Fig. 6 Experimental characteristics and simulation result comparaison. **a** Output characteristics for different bulk traps concentrations for pentacene based-OFET **b** transfer characteristics for different traps energy levels for pentacene based-OFET. **c** Output characteristics for different bulk traps concentrations for Polyera™ N2200 based-OFET **d** transfer characteristics for different traps energy levels for Polyera™ N2200 based-OFET (W/L = 200)
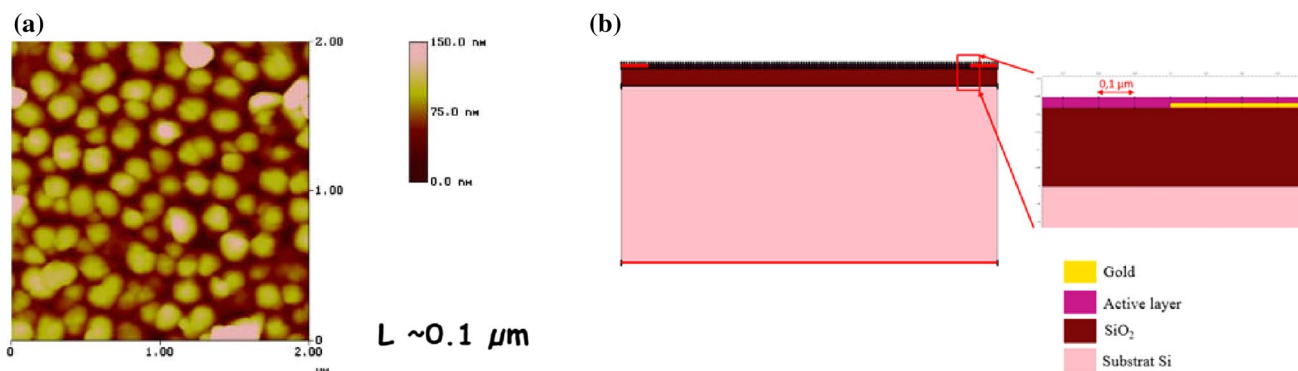

Fig. 7 **a** AFM image of a pentacene thin film deposited by vacuum evaporation **b** simulated transistor structure with grain size equal to 0.1 µm
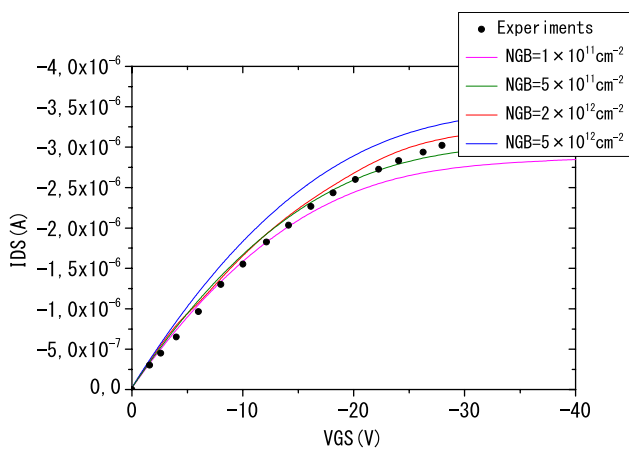
Fig. 8 Output curves of the pentacene based OFET for different densities of interface traps at grain boundaries, W/L = 200

conduction band. We note that the effect of the traps affect more the electrical characteristics in the case of n-type transistor which can explain the limitation of electron transport and low mobility in these types of materials.

Pentacene is a material with morphology characterized by the presence of grains with lateral sizes that vary depending on the deposition parameters or even with the way the surface has been treated prior to evaporation (Fig. 7a). To take into account this effect, the active layer was cut into domains with lateral dimensions equal to 0.1 μm (Fig. 7b) to simulate the interface traps at the grain boundaries. For Polyera[TM] N2200 we will only consider the bulk traps effect. For the same traps energy value (0.2 eV) for the simulated output characteristics with different interface traps densities at the grains boundaries (Fig. 8), we highlight a slight dependence on the current level compared to bulk traps. For a value of $N_{GB} = 5 \times 10^{11}$ cm^{-2},
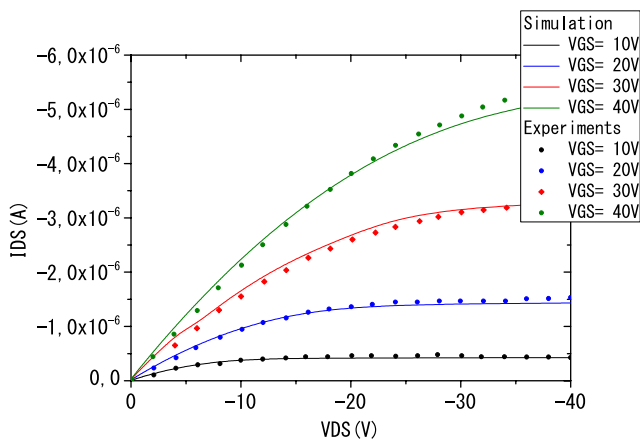
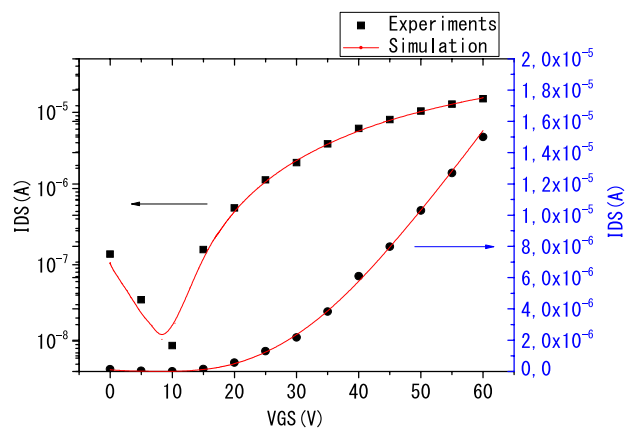**(a)**
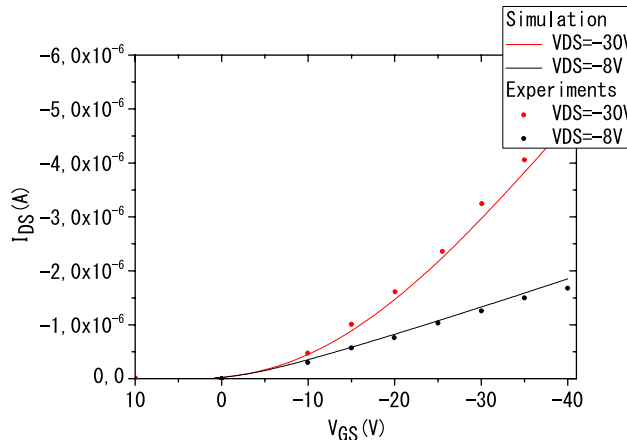
(b)
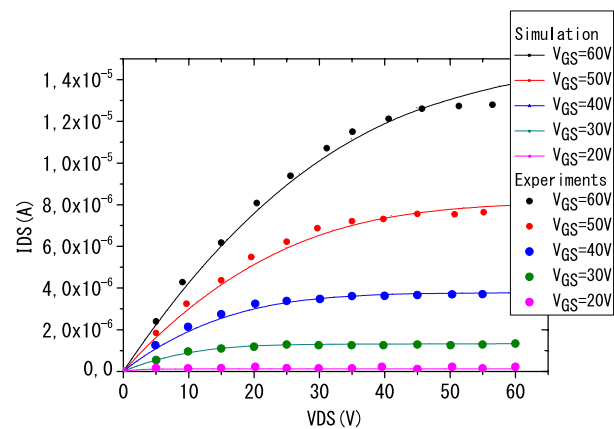
(c)

(d)

Fig. 9 a Transfer characteristics of pentacene based OFETs **b** Output characteristics of pentacene based OFETs **c** Transfer characteristics of Polyera[TM] ActiveInk OFETs **d** Output characteristics of Polyera[TM]

ActiveInk OFETs: experimental (*dotted*) versus TCAD simulation (*solid*) results, W/L = 200
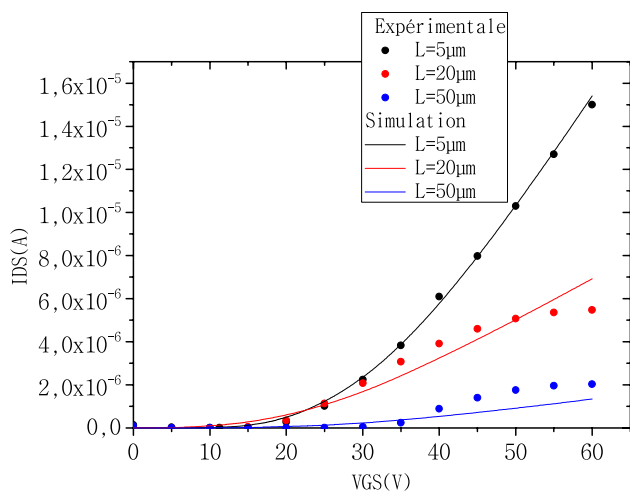
Fig. 10 Transfer characteristics of Polyera™ based OFETs for different channel length, experimental (*dotted*) versus TCAD simulation (*solid*) results

Table 2 Extracted electrical parameters from experiments and simulation data

L (μm)		V_{th} (V)	I_{ON}/I_{OFF}	μ (cm^2 V^{-1} s^{-1})
5 μm	Experiments	10	2.2×10^3	0.05
	Simulation	10	2.8×10^3	0.05
20 μm	Experiments	11.6	10^3	0.048
	Simulation	12	10^3	0.046
50 μm	Experiments	10.1	10^3	0.048
	Simulation	8.8	10^3	0.046

simulations show good agreements with the experimental results. Another study can be realized with the optimization of the grain size to achieve better electrical characteristics. The variation of the grain size can allow us to clearly understand the grain boundary effects on the transport properties of the OTFT.

From the simulation data, we can conclude that electrical characteristics of both n and p-type organic field effect transistors can be properly represented by a single level traps model with respect to the valence band or conduction band, a fixed charges model at the oxide/semiconductor interface, grain boundaries traps effect, and a field-dependent mobility model. With simulated values for one of each parameter we obtain an almost perfect agreement with the experimental data. This is shown in Fig. 9 where we plotted the experimental and simulated electrical characteristics for both types of devices.

To verify our model, we applied our simulation to different devices with different channel length (5, 20, 50 μm) (Fig. 10). The decrease in the transistor channel length

leads to a reduction of the threshold voltage without changing the mobility.

This shift towards negative voltages is due to the fact that in the case of small channel length, the electric field varies much more quickly between the source and the drain. Table 2 summarizes the electrical performances of each transistor. We can conclude that our model is able to reproduce faithfully the experimental characteristics of the studied devices.

3 Conclusion

The important role of device simulations in a better understanding of the material properties and device mechanisms manifests in OFETs based on n and p- type organic materials. This study pegs at comparing current characteristics TCAD simulation and experimental data of pentacene and Polyera™ N2200 based OTFTs realized by our group. The effect of field-dependent mobility, oxide/semiconductor interface fixed charge, bulk traps effects and grain boundaries traps effects were underlined by providing 2D drift–diffusion simulations. In general, we can conclude that device simulations show good agreements with the experimental results.

References

1. D.A. Links, W. Hu, Y. Tao, H. Sirringhaus, "Organic electronics—new physical chemistry insight". Phys. Chem. Chem. Phys. **14**, 14097–14098 (2012)
2. C. Mu, P. Liu, W. Ma, K. Jiang, J. Zhao, K. Zhang, Z. Chen, Z. Wei, Y. Yi, J. Wang, S. Yang, F. Huang, A. Facchetti, H. Ade, H. Yan, "High-effi ciency all-polymer solar cells based on a pair of crystalline low-bandgap polymers". Adv. Mater. **26**, 7224–7230 (2014)
3. J.S. Swensen, E. Polikarpov, A. Von Ruden, L. Wang, L.S. Sapochak, A.B. Padmaperuma, "Improved efficiency in blue phosphorescent organic light- emitting devices using host materials of lower triplet energy than the phosphorescent blue emitter". Adv. Funct. Mater. **21**, 3250–3258 (2011)
4. B.K.C. See, A. Becknell, J. Miragliotta, H.E. Katz, "enhanced response of n-channel naphthalenetetracarboxylic diimide transistors to dimethyl methylphosphonate using phenolic receptors". Adv. Mater. **26**, 3322–3327 (2007)
5. Y. Xu, C. Liu, D. Khim, Y. Noh, "Development of high-performance printed organic field-effect transistors and integrated circuits". Phys. Chem. Chem. Phys. **17**, 26553–26574 (2015)
6. J. Chang, H. Qu, OOI Z.-E., J. Zhang, Z. Chen, J. Wuab, C. Chi, "6,13-Dicyano pentacene-2,3:9,10-bis(dicarboximide) for solution-processed air-stable n-channel field effect transistors and complementary circuit". J. Mater. Chem. C. **1**, 456–462 (2013)
7. B. Hafsi, A. Boubaker, N. Ismaïl, A. Kalboussi, K. Lmimouni, "TCAD simulations of graphene field-effect transistors based on the quantum capacitance effect", J. Korean. Phys. Soc. **67**(7), 1201–1207 (2015)

8. R. Escoffier, W. Fichtner, D. Fokkema, E. Lyumkis, O. Penzin, B. Polsky, A. Schenk, B. Schmithüsen, "DESSIS 10.0 Manual", ISE Integr. Syst. Eng. AG, CH-Zürich **96**, 161 (1996).

9. Y. Roichman, N. Tessler, "Generalized Einstein relation for disordered semiconductors implications for device performance". Appl. Phys. Lett. **80**(11), 1948–1950 (2001)

10. H. Worne, J.E. Anthony, D. Natelson, "Transport in organic semiconductors in large electric fields: From thermal activation to field emission". Appl. Phys. Lett. **96**(053308), 24 (2010)

11. S. D. Ganichev, E. Ziemann, W. Prettl, I. N. Yassievich, A. A. Istratov, E. R. Weber, "Distinction between the Poole-Frenkel tunneling models of electric-field-stimulated carrier emission from deep levels in semiconductors". Phys. Rev.B. **61**(15), 361–365 (2000).

12. E.A. Silinish, V. Cápek, *"Organic molecular crystals their electronic states"*. (Springer Verlag, Berlin, 1980)

13. T. Schuettfort, S. Huettner, S. Lilliu, J.E. MacDonald, L. Thomsen, C.R. McNeill, "Surface and bulk structural characterization of a high-mobility electron-transporting polymer". Macromolecules **44**, 1530–1539 (2011)

14. B.A. Schubert, H. Collins, I.A. Mangold, W. Howard, K. Schindler, S. Vandewal, J. Roland, F. Behrends, R. Kraffert, Z. Steyrleuthner, K. Chen, R. Fostiropoulos, A. Bittl, A. Salleo, F. Facchetti, H.W. Laquai, D. Ade, Neher, "Correlated donor/acceptor crystal orientation controls photocurrent generation in all-polymer solar cells". Adv. Funct. Mater **24**(26), 4068–4081 (2014)

15. R. Brown, C. P. Jarrett, D. M. de Leeuw, M. Matters, "Field-effect transistors made from solution-processed organic semiconductors". Synth. Met. **88**(1), 37–55 (1997).

16. Ellis R, Smith R., *Polymers: a property database*, 2nd edn, (CRC Press, Boca Raton, 2009).

17. L. Sebastian, G. Weiser, H. Bässler, "Charge transfer transitions in solid tetracene and pentacene studied by electroabsorption". Chem. Phys. **61**(1–2), 125–135 (1981)

18. S. Scheinert, G. Paasch, "Fabrication and analysis of polymer field-effect transistors". Phys. Stat. Sol. **1301**(6), 1263–1301 (2004)

19. A. Skaiky, "Elaboration, caractérisation et modélisation de transistors Organiques, à base de pentacène. Application aux circuits électroniques", Phd. thesis, Université de Liomoges, (2013).

20. J.C. Blakesley, M. Schubert, R. Steyrleuthner, Z. Chen, A. Facchetti, D. Neher, "Time-of-flight measurements vertical transport in a high electron-mobility polymer". Appl. Phys. Lett. **99**(18), 183310 (2011)

21. M. Bolognesi, M. Berliocchi, A. Manenti, P. Di Carlo, K. Lugli, C.Dufour Lmimouni,, "Effects of grain boundaries, field-dependent mobility, and interface trap states on the electrical characteristics of pentacene TFT". IEEE Trans. Electron. Devices **51**(12), 1997–2003 (2004)

22. G. J. A. H. Wetzelaer, M. Kuik, Y. Olivier, V. Lemaur, J. Cornil, S. Fabiano, M. A. Loi, P. W. M. Blom, "Asymmetric electron and hole transport in a high-mobility n-type conjugated polymer," Phys. Rev. B—Condens. Matter Mater. Phys. **86**(16), 1–9 (2012).

23. W.L. Kalb, B. Batlogg, "Calculating the trap density of states in organic field-effect transistors from experiment: a comparison of different methods". Phys. Rev. B **8**, 035327 (2009)

24. S. Fonash, Appendix G. "Determining n(x) for the Space-charge-neutral Region of a Heterojunction p-type Bottom Material," Solar cell device physics, Elsevier, 343–345, (2010)

25. IEEE (2004) Standard 1620TM. In: "IEEE standard test methods for the characterization of organic transistors and materials", IEEE, New York, (2004).

26. M. McDowell, I.G. Hill, J.E. McDermott, S.L. Bernasek, J. Schwartz, "Improved organic thin-film transistor performance using novel self-assembled monolayers ". Appl. Phys. Lett. **88**, 073505 (2006)

27. H. Yan, H. Hanagata, H. Okuzaki, "Low-voltage organic complementary inverters fabricated with pentacene/$SrTiO_3$ and C_{60}/$SrTiO_3$ field-effect transistors". Eur. Phys. J. Appl. Phys. **61**(3), 30201 (2013)

28. M. Sharifi A. Bazyar, "Pentacene-based organic field-effect transistors: analytical model and simulation methods versus experiment data". ACEEE Int. J. Control Syst. Instrum. **02**(03), 3–7 (2011)

29. Di Carlo, A. Bolognesi, M. Berliocchi, P. Lugli, "The interplay between barrier contact, mobility models and traps in the electrical characteristics of OTFT". Org. Field Eff. Transistors, **5217**, 87–94 (2003).